Thickness-Dependent Polarization of Strained $BiFeO_3$ Films with Constant Tetragonality

J. E. Rault,[1] W. Ren,[2,3] S. Prosandeev,[2] S. Lisenkov,[4] D. Sando,[5] S. Fusil,[5,6] M. Bibes,[5] A. Barthélémy,[5] L. Bellaiche,[2] and N. Barrett[1,*]

[1]*CEA, DSM/IRAMIS/SPCSI, F-91191 Gif-sur-Yvette Cedex, France*
[2]*Physics Department and Institute for Nanoscience and Engineering, University of Arkansas, Fayetteville, Arkansas 72701, USA*
[3]*Department of Physics, Shanghai University, 99 Shangda Road, Shanghai 200444, China*
[4]*Department of Physics, University of South Florida, 4202 East Fowler Avenue, Tampa, Florida 33620-5700, USA*
[5]*Unité Mixte de Physique CNRS/Thales, 1 Avenue Augustin Fresnel, Campus de l'Ecole Polytechnique, 91767 Palaiseau, France and Université Paris-Sud, 91405 Orsay, France*
[6]*Université d'Evry-Val d'Essonne, Boulevard François Mitterrand, 91025 Evry cedex, France*
(Received 17 May 2012; published 26 December 2012)

We measure the ferroelectric polarization of $BiFeO_3$ films down to 3.6 nm using low energy electron and photoelectron emission microscopy. The measured polarization decays strongly below a critical thickness of 5–7 nm predicted by continuous medium theory whereas the tetragonal distortion does not change. We resolve this apparent contradiction using first-principles-based effective Hamiltonian calculations. In ultrathin films, the energetics of near open circuit electrical boundary conditions, i.e., an unscreened depolarizing field, drive the system through a phase transition from single out-of-plane polarization to nanoscale stripe domains. It gives rise to an average polarization close to zero as measured by the electron microscopy while maintaining the relatively large tetragonal distortion imposed by the nonzero polarization state of each individual domain.

DOI: 10.1103/PhysRevLett.109.267601 PACS numbers: 77.80.−e, 68.37.Xy, 77.55.fp

A major issue for prospective nanoscale, strain-engineered [1] ferroelectric devices [2] is the decrease of the polarization P_r of ultrathin films. The depolarizing field arising from uncompensated surface charges reduces or even suppresses ferroelectricity below a critical thickness [3,4]. Ferroelectric capacitors, for example, may exhibit a critical thickness [5,6]. Lichtensteiger *et al.* [7] have shown that the decrease in P_r in $PbTiO_3$ (PTO) thin films between 20 and 2.4 nm on Nb-doped $SrTiO_3$ (STO) substrates is concomitant with that of the tetragonality [ratio of the out-of-plane to in-plane lattice parameter c/a)]. On $La_{0.67}Sr_{0.33}MnO_3$ (LSMO), PTO polydomains were formed below 10 nm with high tetragonality [8]. The formation of a polydomain state has been suggested for $SrRuO_3/Pb(Zr, Ti)O_3/SrRuO_3$ capacitors with $Pb(Zr, Ti)O_3$ thicknesses below 15 nm [9]. Pertsev and Kohlstedt showed the importance of misfit strain for the critical thickness of the monodomain-polydomain stability for PTO and $BaTiO_3$ [10]. Using piezoresponse force microscopy (PFM), $BiFeO_3$ (BFO) films have been shown to remain ferroelectric down to a few unit cells [11–13] with both the polarization and the slope of the piezoresponse hysteresis loop scaling with tetragonality. However, PFM is very local and can only provide indirect, semiquantitative estimates of the polarization. Imperfect tip surface contact can contribute to polarization suppression via the depolarizing field. Direct electrical measurements of the polarization-field [$P(E)$] loop in ultrathin ferroelectric films are a challenge because of leakage current for thicknesses below a few tens of nm [11,14]. They become impossible in the tunneling regime for ultrathin films (5 nm or less) which, furthermore, is of the same order as the critical thickness, h_{eff}, estimated from Landau-Ginzburg-Devonshire (LGD) elastic theory for polarization stability [13,15]. BFO can accommodate in-plane compressive strain via out-of-plane extension and through oxygen octahedron rotation about $\langle 111 \rangle$ [16], a degree of freedom not available in $P4mm$ PTO films. This interplay between strain, tetragonality, and octahedra rotations leads to an unexpected decrease of T_C with strain, at odds with the variation of c/a ratio. Thus the relationship between structural parameters and the remnant out-of-plane polarization in very thin films remains an open question.

In this Letter, we have studied the polarization of BFO films from 70 to 3.6 nm thick using a combination of x-ray diffraction (XRD), mirror electron microscopy (MEM) and photoelectron emission microscopy (PEEM). The electron microscopy techniques provide full-field imaging of the electrostatic potential above the surface and the work function whereas the tetragonality is measured by XRD. The results are interpreted in light of a three-dimensional (3D) generalization of a previously developed dead layer model for thin films within the framework of continuous medium theory that predicts a fast decrease of the polarization when decreasing the thickness. Interestingly, the extremely low polarization below h_{eff} does not scale with the tetragonality and is explained using first principles-based effective Hamiltonian calculations which show that as a function of screening the films undergo a phase

transition from single to nanoscale stripe domains with an overall out-of-plane polarization close to zero.

Bilayers of BFO and LSMO were epitaxially grown on (001)-oriented STO substrates by pulsed laser deposition using a frequency tripled ($h\nu = 355$ nm) Nd-doped yttrium aluminium garnet (Nd:YAG) laser at a frequency of 2.5 Hz [11]. The 20 nm thick LSMO layer serves as a metallic bottom electrode for ferroelectric characterization. XRD measurements on 70 to 3.6 nm-thick thin films were performed to track the out-of-plane parameter and c/a ratio [Fig. 1(a)]. The c/a increases slightly from 1.050 for the 70 nm film to 1.053 for 7 nm, then remains constant down to 3.6 nm. This contrasts dramatically with the behavior of PTO reported in Ref. [7] where c/a decreases with thickness. The chemistry of the films was measured by x-ray photoelectron spectroscopy (XPS). Figure 1(b) shows spectra from a Bi $4f$ core level for the thickest (70 nm) and thinnest (3.6 nm) films. The spectra are virtually identical for both films (for intermediate thicknesses, see Supplemental Material [17]) showing that the chemical state and stoichiometry do not change. Bi $4f$ spectra have a thickness *independent* component shifted by 0.6 eV to higher binding energy, suggesting that our strained thin films do not exhibit the several nanometer thick skin observed on single crystals [18]. C 1s spectra show that contamination of the BFO surface is similar for every thickness suggesting a similar contribution to extrinsic screening in all films [17].

For the 70 nm BFO film, the ferroelectric properties were investigated by standard polarization versus electric field $P(E)$ loops [Fig. 1(c)]. The piezoresponse hysteresis loops are shown in Fig. 1(d). They are position independent and exhibit similar coercive values as nonlocal $P(E)$ loops, attesting to sample homogeneity. In a (001) BFO film, P^+ and P^- states are the projections of ⟨111⟩ polarization along [001]. Poling of micron sized domains was performed by applying a dc voltage higher than the coercive voltage (inferred from the piezoresponse loops) on the tip while the bottom electrode was grounded. PFM imaging was carried out at an excitation frequency of 4–7 kHz and an ac voltage of 1 V. No morphology change occurred during poling as checked by atomic force microscopy. A low-energy electron microscope (LEEM, Elmitec GmbH) was used to measure the electron kinetic energy of the MEM (reflected electrons)-LEEM (backscattered electrons) transition with a spatial resolution of 30 nm. The transition energy is a measure of electrostatic potential just above the sample surface [19] and depends on polarization and the screening of polarization-induced surface charge [20]. It allows a noncontact estimation of the out-of-plane polarization for tunneling films, otherwise inaccessible to standard electrical methods. All experiments were done at least two days after domain writing to ensure that the observed contrast is not due to residual injected charges.

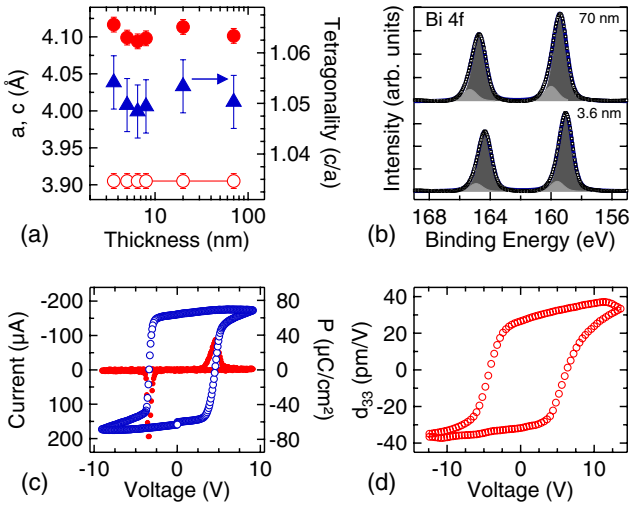

FIG. 1 (color online). (a) Evolution of pseudocubic lattice parameters a and c, and c/a ratio with thickness. (b) Bi $4f$ spectra for 70 and 3.6 nm films showing two components (surface in light grey, bulk in dark grey) for each spin-orbit core-level. (c) Polarization-voltage and current-voltage hysteresis loop of BFO (70 nm)/LSMO (20 nm)//STO (001). (d) Piezoresponse hysteresis loop (local measurement under the PFM tip).

Figure 2(b) shows a typical LEEM image with a field of view of 33 μm for incident electron energy (E_{inc}) of 1.40 eV. The observed contrast reproduces well the PFM image of Fig. 2(a). A full image series across the MEM-LEEM transition (E) was acquired by varying E_{inc} from -2.0 to 3.0 eV. Figure 3(a) displays the electron reflectivity curves showing the MEM (high reflectivity) to LEEM (low reflectivity) transition for the P^+ (brown upwards triangles, $E = 0.75$ eV) and P^- (green downwards triangles, $E = 1.20$ eV) domains. Using complementary error function fits we obtain MEM-LEEM transition maps showing clear contrast in the electrostatic potential above the surface between the P^+, P^-, and unwritten regions [Fig. 3(b)].

The energy filtered PEEM experiments used a NanoESCA X-PEEM (Omicron Nanotechnology GmbH). PEEM of the photoemission threshold gives a direct, accurate (± 20 meV), and nondestructive map of the work function [21] that may depend, for example, on domain polarization [22]. Image series were acquired over the photoemission threshold region with a mercury lamp excitation ($h\nu = 4.9$ eV). The lateral resolution was

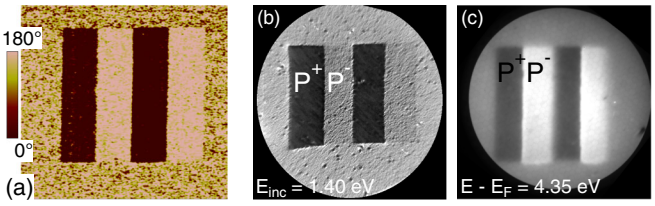

FIG. 2 (color online). (a) PFM phase image of written P^+/P^- domains. Each domain is 5×20 μm^2. (b) LEEM image for $E_{\mathrm{inc}} = 1.40$ eV. (c) PEEM image at $E - E_F = 4.35$ eV.

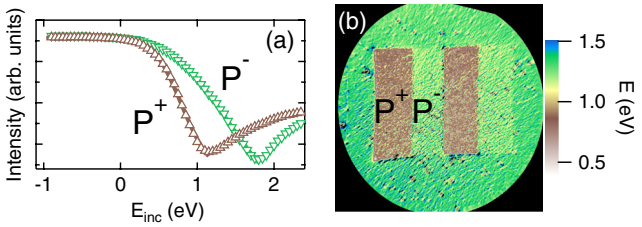

FIG. 3 (color online). (a) Reflectivity spectra extracted from the P^+ and P^- domains. (b) MEM-LEEM transition map obtained from the image series (70 nm thin film).

estimated to be 200 nm and energy resolution 200 meV. Figure 2(c) shows a typical PEEM image of the prepoled P^+ and P^- regions for the 70 nm BFO film. The energy contrast between oppositely polarized domains fits the PFM image except at the domain boundary where the lateral electric field induced by a P^+/P^- domain wall deflects electrons [23]. We extract the threshold from the pixel-by-pixel spectra using an error function to model the rising edge of the photoemission [Fig. 4(a)]. Figure 4(b) maps the work function in the P^+, P^-, and as-grown regions.

The difference in the MEM-LEEM transition of the P^+ and P^- regions, ΔE, varies from 450 meV for the 70 nm film to 25 meV for the 3.6 nm film and is plotted in Fig. 5(a) (black circles, right axis). The mean work function difference measured in PEEM between P^+ and P^- domains, $\Delta\Phi_F = \Phi_F(P^+) - \Phi_F(P^-)$, is plotted as a function of thickness in Fig. 5(a) (left axis). While $\Delta\Phi_F$ is 300 meV between 70 and 7 nm, between 7 and 5 nm it drops to 20 meV.

The polarization charges at the BFO surface are screened over a so-called dead layer leading to an inward (P^+) or outward (P^-) surface dipole. By measuring the work function (or surface potential) *difference* between two opposite domains, our method allows a direct measurement of the polarization-induced dipoles since any averaged nonferroelectric contribution is canceled. The surface dipole difference, hence the surface potential and work function difference, is proportional to the difference in polarization charges when going from the P^+ to the P^- domains:

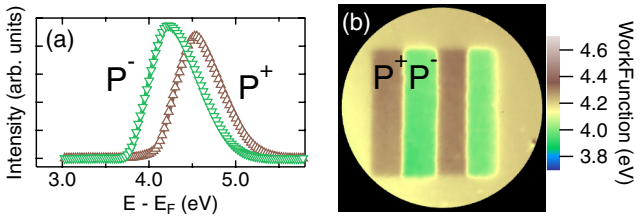

FIG. 4 (color online). (a) Threshold spectra extracted from P^+ and P^- domains. (b) Work function map obtained from the threshold image series (70 nm thin film).

$$\Delta\Phi_F, \Delta E \propto \frac{e}{\epsilon_0}(P^+ \cdot d^+ - P^- \cdot d^-) \approx 2\frac{e}{\epsilon_0}P_r \cdot d, \quad (1)$$

where $P^{+,-}$ and $d^{+,-}$ are the polarization and dead layer thickness for the upward, downward domains; P_r is the average magnitude of the polarization in the two poled domains and d is the average dead layer thickness. For the sake of generality, one can take into account electronic screening via a high-frequency dielectric permittivity, but it would still leave a linear relation between polarization and $\Delta\Phi_F$, ΔE. $P_z/P_{\max}$, where P_z is the measured out-of-plane polarization and $P_{\max}$ the value for the 70 nm film, is plotted as a function of film thickness in Fig. 5(b). By comparison with Fig. 1(a), the drop of average polarization between 7 and 5 nm does not result from a decrease in the c/a ratio, contrary to PTO thin films [7]. Here the c/a ratio increases for thinner films and is constant at 1.054 below 5 nm. If there were no polarization then it should be about 1.03. However, PTO is almost fully relaxed whereas BFO is compressively strained. Secondly, in BFO, the polarization deviates appreciably from the [001] direction and is the macroscopic average of four ⟨111⟩ type distortions. We have therefore generalized the 1D dead layer LGD model of Bratkovsky and Levanyuk [15] to the 3D polarization case. It gives the following relation for thickness dependence of polarization [17]:

$$\frac{P_z}{P_{\max}} = A\sqrt{B + \sqrt{1 - \frac{h_{\text{eff}}}{h}}}, \quad (2)$$

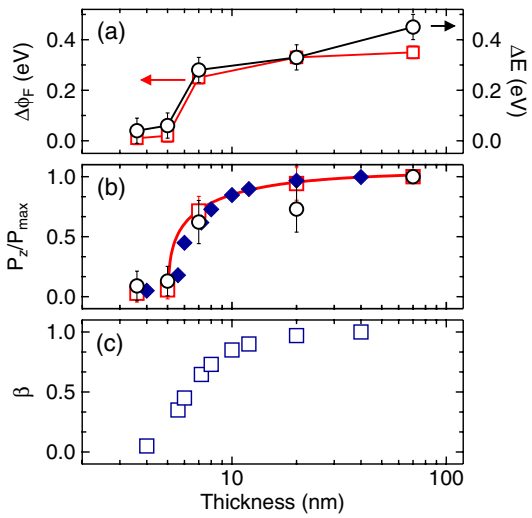

FIG. 5 (color online). Thickness dependence of (a) $\Delta\Phi_F$ (red squares) and ΔE (black circles). (b) $P_z/P_{\max}$ calculated from PEEM (red squares) and MEM-LEEM (black circles). Red curve is fit to PEEM and LEEM data with $h_{\text{eff}} = 5.6$ nm. Blue diamonds are $P_z/P_{\max}$ values used for numerical simulations. (c) Screening coefficient β calculated from experimental $P_z/P_{\max}$ values.

where h_{eff} is the effective thickness below which the macroscopic P_z goes to zero, and A, B are fitting parameters. A good fit to the data is obtained with $h_{\mathrm{eff}} = 5.6$ nm [see Fig. 5(b), red curve], compared with 2.4 nm for PTO.

To understand why the measured polarization suddenly drops in ultrathin strained (001) BFO films, while the axial ratio is still very large, we have conducted first-principles-based, effective Hamiltonian calculations [24–26] that take into account free surfaces [24]. We used the lattice parameter of the STO substrate for the pseudocubic in-plane lattice constant of BFO, leading to a misfit strain of -1.8%, in agreement with the experimental value. The calculation includes the local electric dipoles, the strain tensor, and tilting of the oxygen octahedra. The electrical boundary conditions are governed by a coefficient denoted as β described in Ref. [27]. Practically, β can vary between 0 (ideal open-circuit, maximal depolarizing field) and $\beta = 1$ (ideal short-circuit, fully screened depolarizing field). To determine β for each of our grown films we first extract the P_z/P_{max} values from a B-spline interpolation of the experimental data [Fig. 5(b), blue diamonds] and then vary β in the calculations until the predicted P_z/P_{max} perfectly agrees with the experimentally extracted one. Figure 5(c) shows the resulting β values. β decreases with thickness, indicating that the observed decrease of polarization is related to imperfect screening of the depolarizing field. The vanishing of the overall z component of the polarization [which occurs experimentally for thicknesses lower than 5.6 nm, see Fig. 5(b)] is associated with values of β lower than 0.4 [see Fig. 5(c)].

To understand what happens for these β values, we performed additional first-principles-based effective Hamiltonian calculations on a single $20 \times 20 \times 20$ supercell (i.e., with a thickness of 8 nm) allowing β to vary. This supercell was chosen because around 8 nm the polarization is very sensitive to the thickness [Fig. 5(b)]. The results are shown in Fig. 6. At a critical value of β of 0.275 ± 0.025

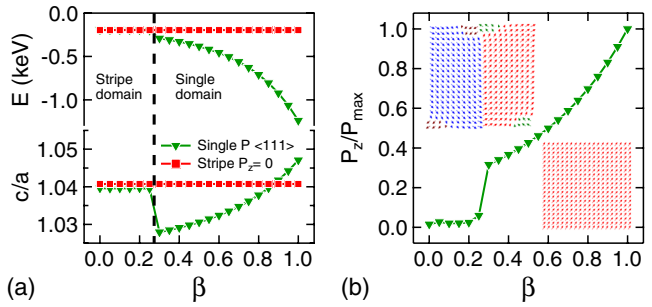

FIG. 6 (color online). (a) (top panel) Slab energy with β showing a transition from a single domain (out-of-plane polarization, green triangles) to stripe domains (no total out-of-plane polarization, red squares) below $\beta_{\mathrm{crit}} = 0.30$. (bottom panel) Theoretical c/a ratio with β for the two phases. (b) Evolution of P_z/P_{max} with β. Inset: Domain morphology (upper left, stripe domains; bottom right, single domain). All these data are for a $20 \times 20 \times 20$ slab, i.e., a film with a thickness of 8 nm.

the BFO supercell goes from a phase with a uniform out-of-plane polarization to a stripe domain phase with a vanishing overall out-of-plane polarization. Figure 6(a) displays the energy of these two phases as a function of β. The monodomain phase is energetically more favorable than the stripe nanodomains for β above 0.30 and less for smaller β values. The predicted evolution of the c/a ratio, and of the overall P_z/P_{max}, with β for single and stripe domain phases are shown in Figs. 6(a) and 6(b), respectively. Interestingly, a continuous ferroelectric to paraelectric transition would lead to a large monotonic decrease of tetragonality [Fig. 6(a), green triangles], which we do not measure below h_{eff}. Rather, the transformation from ferroelectric monodomains to nanostripe domains leads to a (large) c/a similar to the one associated with short-circuit-like conditions (i.e., for which β is close to 1). Such results are consistent with our experimental findings that c/a does not vary between 70 and 3.6 nm, and explains that such insensitivity to strain is likely due to the formation of nanostripe domains. The single to stripe domain transition explains the loss of contrast in electronic microscopy observed in LEEM and PEEM contrast between 7 and 5 nm, because these regions do not possess any overall z component of the polarization. The stripes have a typical dimension of a few nanometers, which is below the lateral resolution of our experiments. [The top left inset of Fig. 6(b) shows the morphology of these domains.] However, stripe domains in BFO thin films close to the h_{eff} value have been observed by PFM [28]. For such thin films, one might also ask to what extent the screening at the LSMO and BFO interface affects the measured polarization. Transmission electron microscopy of the interface between LSMO and a 3.2 nm BFO film suggests that the first three BFO unit cells are screened by the interface charge [29]. This also fits nicely with our experimental observation of an abrupt decrease in polarization starting at 7 nm, 1.4 nm above the calculated h_{eff}.

In summary, we have measured the polarization in ultrathin strained (001) BFO films using PEEM and LEEM. The polarization drops abruptly below a critical thickness h_{crit} whereas the tetragonality has a high constant value. A first-principles-based effective Hamiltonian approach suggests that BFO exhibits a first order phase transition to stripe domains at $h_{\mathrm{crit}} = 5.6$ nm, corresponding to a screening factor, β, below 0.35. This model fits the experimental measurement of the average polarization and the c/a ratio.

J. R. is funded by a CEA Ph.D. grant CFR. This work was supported by the ANR projects "Meloïc", "Nomilops" and "Multidolls". W. R. acknowledges the Eastern Scholar Professorship at Shanghai Institutions of Higher Education, Shanghai Municipal Education Commission, and support from National Natural Science Foundation of China under Grant No. 11274222. L. B. thanks the financial support of ARO Grant No. W911NF-12-1-0085, and ONR Grants No. N00014-11-1-0384,

No. N00014-12-1-1034, and No. N00014-08-1-091. We also acknowledge DOE, Office of Basic Energy Sciences, under Contract No. ER-46612 and NSF Grants No. DMR-1066158 and No. DMR-0701558, for discussions with scientists sponsored by these grants. Some computations were made possible thanks to the MRI Grant No. 0722625 (NSF), the ONR Grant No. N00014-07-1-0825 (DURIP) and a Challenge grant (DOD). We thank E. Jacquet, C. Carrétéro and H. Béa for assistance in sample preparation; K. Winkler, B. Krömker (Omicron Nanotechnology), C. Mathieu, D. Martinotti for help with the PEEM and LEEM experiments; and P. Jégou for the XPS measurements.

*To whom all correspondence should be addressed.
nick.barrett@cea.fr

[1] K. J. Choi, M. Biegalski, Y. L. Li, A. Sharan, J. Schubert, R. Uecker, P. Reiche, Y. B. Chen, X. Q. Pan, V. Gopalan, L. Q. Chen, D. G. Schlom, and C. B. Eom, Science **306**, 1005 (2004).
[2] M. Bibes, Nat. Mater. **11**, 354 (2012).
[3] G. Gerra, A. K. Tagantsev, N. Setter, and K. Parlinski, Phys. Rev. Lett. **96**, 107603 (2006).
[4] J. Junquera and P. Ghosez, Nature (London) **422**, 506 (2003).
[5] D. J. Kim, J. Y. Jo, Y. S. Kim, Y. J. Chang, J. S. Lee, J. G. Yoon, T. K. Song, and T. W. Noh, Phys. Rev. Lett. **95**, 237602 (2005).
[6] A. Petraru, H. Kohlstedt, U. Poppe, R. Waser, A. Solbach, U. Klemradt, J. Schubert, W. Zander, and N. A. Pertsev, Appl. Phys. Lett. **93**, 072902 (2008).
[7] C. Lichtensteiger, J. M. Triscone, J. Junquera, and P. Ghosez, Phys. Rev. Lett. **94**, 047603 (2005).
[8] C. Lichtensteiger, M. Dawber, N. Stucki, J. M. Triscone, J. Hoffman, J. Yau, C. H. Ahn, L. Despont, and P. Aebi, Appl. Phys. Lett. **90**, 052907 (2007).
[9] V. Nagarajan, J. Junquera, J. Q. He, C. L. Jia, R. Waser, K. Lee, Y. K. Kim, S. Baik, T. Zhao, R. Ramesh, P. Ghosez, and K. M. Rabe, J. Appl. Phys. **100**, 051609 (2006).
[10] N. A. Pertsev and H. Kohlstedt, Phys. Rev. Lett. **98**, 257603 (2007).
[11] H. Béa, S. Fusil, K. Bouzehouane, M. Bibes, M. Sirena, G. Herranz, E. Jacquet, J. P. Contour, and A. Barthélémy, Jpn. J. Appl. Phys. **45**, L187 (2006).
[12] Y. H. Chu, T. Zhao, M. P. Cruz, Q. Zhan, P. L. Yang, L. W. Martin, M. Huijben, C. H. Yang, F. Zavaliche, H. Zheng, and R. Ramesh, Appl. Phys. Lett. **90**, 252906 (2007).
[13] P. Maksymovych, M. Huijben, M. Pan, S. Jesse, N. Balke, Y. H. Chu, H. J. Chung, A. Y. Borisevich, A. P. Baddorf, G. Rijnders, D. H. A. Blank, R. Ramesh, and S. V. Kalinin, Phys. Rev. B **85**, 014119 (2012).
[14] D. H. Kim, H. N. Lee, M. D. Biegalski, and H. M. Christen, Appl. Phys. Lett. **92**, 012911 (2008).
[15] A. M. Bratkovsky and A. P. Levanyuk, Phys. Rev. Lett. **84**, 3177 (2000).
[16] I. C. Infante, S. Lisenkov, B. Dupé, M. Bibes, S. Fusil, E. Jacquet, G. Geneste, S. Petit, A. Courtial, J. Juraszek, L. Bellaiche, A. Barthélémy, and B. Dkhil, Phys. Rev. Lett. **105**, 057601 (2010).
[17] See Supplemental Material at http://link.aps.org/supplemental/10.1103/PhysRevLett.109.267601 for PFM, PEEM, LEEM, and XPS data for all thicknesses and the 3D LDG theoretical development.
[18] X. Martí, P. Ferrer, J. Herrero-Albillos, J. Narvaez, V. Holy, N. Barrett, M. Alexe, and G. Catalan, Phys. Rev. Lett. **106**, 236101 (2011).
[19] S. Cherifi, R. Hertel, S. Fusil, H. Béa, K. Bouzehouane, J. Allibe, M. Bibes, and A. Barthélémy, Phys. Status Solidi RRL **4**, 22 (2010).
[20] I. Krug, N. Barrett, A. Petraru, A. Locatelli, T. O. Mentes, M. A. Nio, K. Rahmanizadeh, G. Bihlmayer, and C. M. Schneider, Appl. Phys. Lett. **97**, 222903 (2010).
[21] C. Mathieu, N. Barrett, J. Rault, Y. Y. Mi, B. Zhang, W. A. de Heer, C. Berger, E. H. Conrad, and O. Renault, Phys. Rev. B **83**, 235436 (2011).
[22] N. Barrett, J. Rault, I. Krug, B. Vilquin, G. Niu, B. Gautier, D. Albertini, P. Lecoeur, and O. Renault, Surf. Interface Anal. **42**, 1690 (2010).
[23] S. A. Nepijko, N. N. Sedov, and G. Schönhense, J. Microsc. **203**, 269 (2001).
[24] S. Prosandeev, S. Lisenkov, and L. Bellaiche, Phys. Rev. Lett. **105**, 147603 (2010).
[25] D. Albrecht, S. Lisenkov, W. Ren, D. Rahmedov, I. A. Kornev, and L. Bellaiche, Phys. Rev. B **81**, 140401 (2010).
[26] I. A. Kornev, S. Lisenkov, R. Haumont, B. Dkhil, and L. Bellaiche, Phys. Rev. Lett. **99**, 227602 (2007).
[27] I. Ponomareva, I. I. Naumov, I. Kornev, H. Fu, and L. Bellaiche, Phys. Rev. B **72**, 140102 (2005).
[28] G. Catalan, H. Bea, S. Fusil, M. Bibes, P. Paruch, A. Barthélémy, and J. F. Scott, Phys. Rev. Lett. **100**, 027602 (2008).
[29] H. J. Chang, S. V. Kalinin, A. N. Morozovska, M. Huijben, Y. Chu, P. Yu, R. Ramesh, E. A. Eliseev, G. S. Svechnikov, S. J. Pennycook, and A. Y. Borisevich, Adv. Mater. **23**, 2474 (2011).